PERGAMON

Micron 31 (2000) 571–580

micron

www.elsevier.com/locate/micron

EELS analysis of cation valence states and oxygen vacancies in magnetic oxides

Z.L. Wang*, J.S. Yin, Y.D. Jiang

School of Materials Science and Engineering, Georgia Institute of Technology, Atlanta, GA 30332-0245, USA

Dedicated to Professor K.H. Kuo on the occasion of his 75th birthday

Abstract

Transition metal oxides are a class of materials that are vitally important for developing new materials with functionality and smartness. The unique properties of these materials are related to the presence of elements with mixed valences of transition elements. Electron energy-loss spectroscopy (EELS) in the transmission electron microscope is a powerful technique for measuring the valences of some transition metal elements of practical importance. This paper reports our current progress in applying EELS for quantitative determination of Mn and Co valences in magnetic oxides, including valence state transition, quantification of oxygen vacancies, refinement of crystal structures, and identification of the structure of nanoparticles.

Keywords: Electron energy-loss spectroscopy; Cation valence states; Oxygen vacancies; Magnetic oxides; White line; Transition metal element

1. Introduction

Transition and rare earth metal oxides are the fundamental ingredients for the advanced smart and functional materials. Many functional properties of inorganic materials are determined by the elements with *mixed valences* in the structure unit (Wang and Kang, 1998), by which we mean that an element has two or more different valences while forming a compound. The discovery of high-temperature superconductors is a successful example of the mixed valence chemistry, and the colossal magnetoresistivity (CMR) (von Helmolt et al., 1994; Jin et al., 1994) observed in the perovskite structured $La_{1-x}A_xMnO_3$ (A = Ca, Sr, or Ba) is another example. Transition and rare earth metal elements with mixed valences are mandatory for these materials to stimulate electronic, structural and/or chemical evolution, leading to specific functionality.

The valence states of metal cations in such materials can certainly be chemically determined using the redox titration, but it is inapplicable to nanophase or nanostructured materials such as thin films. The wet chemistry approaches usually do not provide any spatial resolution. X-ray photoelectron spectroscopy (XPS) can provide information on the average distribution of cation valences for nanostructured materials with certain spatial resolution, but the spatial resolution is nowhere near the desired nanometer scale, and the information provided is limited to a surface layer of 2–5 nm in thickness.

Electron energy-loss spectroscopy (EELS), a powerful technique for materials characterization at a nanometer spatial resolution, has been widely used in chemical microanalysis and the studies of solid state effects (Egerton, 1996). In EELS, the L ionization edges of transition-metal and rare-earth elements usually display sharp peaks at the near-edge region, which are known as *white lines*. For transition metals with unoccupied 3d states, the transition of an electron from 2p state to 3d levels leads to the formation of white lines. The L_3 and L_2 lines are the transitions from $2p^{3/2}$ to $3d^{3/2}3d^{5/2}$ and from $2p^{1/2}$ to $3d^{3/2}$, respectively, and their intensities are related to the unoccupied states in the 3d bands (Pease et al., 1986; Krivanek and Paterson, 1990).

Numerous EELS experiments have shown that a change in valence state of cations introduces a dramatic change in the ratio of the white lines, leading to the possibility of identifying the occupation number of 3d orbital using EELS. Morrison et al. (1985) have applied this technique to study the valence modulation in Fe_xGe_{1-x} alloy as a function of Ge doping. The 3d and 4d occupations of transition and rare earth elements have been studied systematically (Pearson et al., 1988, 1993; Kurata and Colliex, 1993). The crystal structure of a new compound $Mn_{7.5}Br_3O_{10}$ has been refined in reference to the measured Mn valences (Mansot et al., 1994). The oxidation states of Ce and Pr

* Corresponding author. Tel.: +1-404-894-8008; fax: +1-404-894-9140.
E-mail address: zhong.wang@mse.gatech.edu (Z.L. Wang).

0968-4328/00/$ - see front matter
PII: S0968-4328(99)00139-0

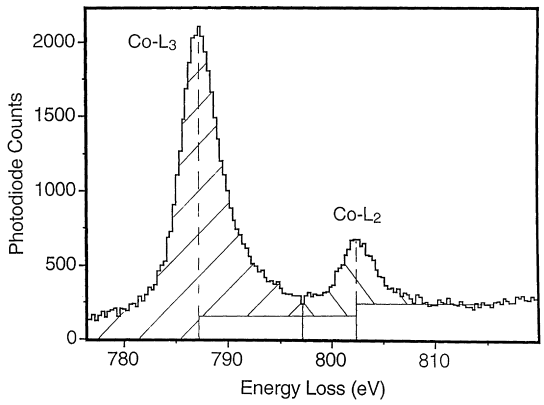

Fig. 1. An EELS spectrum acquired from a Co oxide, showing the technique used to extract the intensities of white lines.

have been determined in an orthophosphate material, in which the constituents of Ce and Pr are in the order of 100 ppm (Fortner and Buck, 1996). Lloyd et al. (1995) and Yuan et al. (1994) have demonstrated the sensitivity of the Fe white lines to the magnetic momentum of the Fe layers.

In this paper, we review our current progresses made in applying EELS for the quantitative determination of the valence states of Mn and Co oxides. The fundamental experimental approach is given first. The applications of EELS will be demonstrated for quantifying the valence transition in Mn and Co oxides, determining the concentration of oxygen vacancies, refining the crystal structure of an anion deficient perovskite, and identifying the crystal structure of nanoparticles (CoO and Co_3O_4).

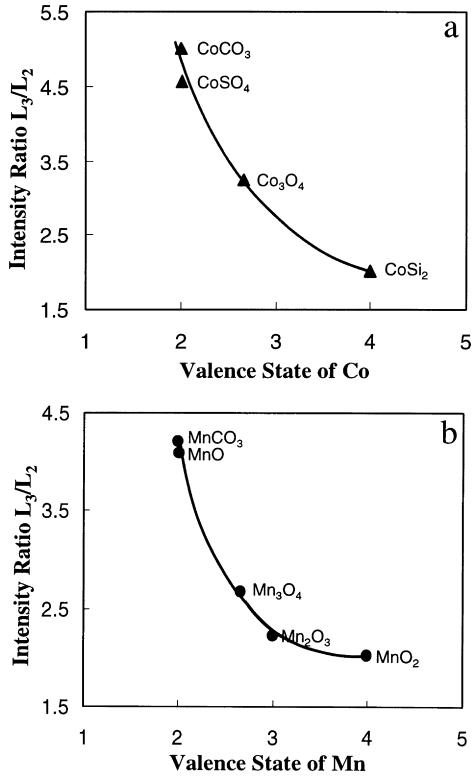

Fig. 2. Plots of the intensity ratios of L_3/L_2 calculated from the spectra acquired from: (a) Co compounds; and (b) Mn compounds as a function of the cation valence. A nominal fit of the experimental data is shown by a solid curve.

2. Principle of EELS measurements

Fig. 1 shows an EELS spectrum of Co oxide acquired at 200 kV using a Hitachi HF-2000 transmission electron microscope equipped with a Gatan 666 parallel-detection electron energy-loss spectrometer. The EELS spectra were acquired in the image mode at a magnification of 40–100 K depending on the required spatial resolution and signal intensity. The EELS data must also be processed first to remove the gain variation introduced by the detector channels. A low-loss valence spectrum and the corresponding core-shell ionization edge EELS spectrum were acquired consecutively from the same specimen region. The low energy-loss spectrum was used to remove the multiple-inelastic-scattering effect in the core-loss region using the Fourier ratio technique. Consequently, the data presented here are the results of single inelastic scattering.

Several techniques have been proposed to correlate the observed EELS signals with the valence states, the ratio of white lines, the normalized white line intensity in reference to the continuous state intensity located ~50–100 eV beyond the energy of the L_2 line, and the absolute energy shift of the white lines. In this study, we use the white line intensity ratio that is calculated using a method demonstrated in Fig. 1 (Pearson et al., 1988, 1993). The background intensity was modeled by step functions in the threshold regions. A straight line over a range of approximately 50 eV was fit to the background intensity immediately following the L_2 white line. This line was then modified into a double step of the same slope with onsets occurring at the white-line maxima. The ratio of the step heights is chosen to be 2:1 in accordance with the multiplicity of the initial states (four $2p_{3/2}$ electrons and two $2p_{1/2}$ electrons) (Kurata and Colliex, 1993; Pearson et al., 1993; Botton et al., 1995; Lloyd et al., 1995). Although there exist some disagreements in literature about the calculation of the normalized white line intensity because the theory behind the white line and their continuos background is rather complex (Thole and van der Laan, 1988), it appears, based on our experience, that the ratio of the white line intensities is likely to be a reliable and sensitive approach. This background subtraction procedure is followed consistently for all of the acquired spectra. The calculated result of L_3/L_2 is rather stable and is not sensitive to the specimen thickness nor the noise level in the spectrum.

EELS analysis of valence state is carried out in reference to the spectra acquired from standard specimens with known cation valence states. Since the intensity ratio of L_3/L_2 is sensitive to the valence state of the corresponding element,

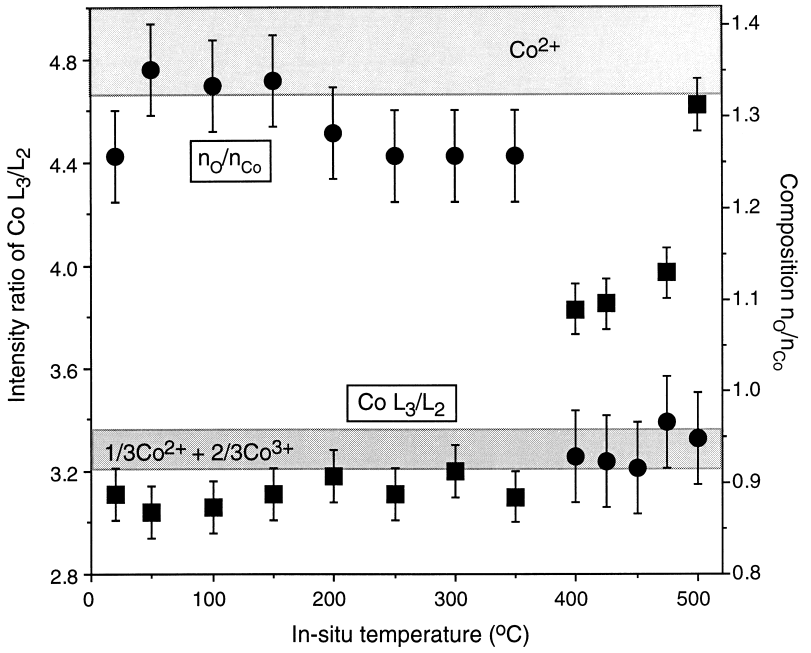

Fig. 3. An overlapped plot of the white line intensity ratio of Co L_3/L_2 and the corresponding chemical composition of n_O/n_{Co} as a function of the in situ temperature of the Co_3O_4 specimen showing the abrupt change in valence state and oxygen composition at 400°C. The error bars are determined from the errors introduced in background subtraction and data fluctuation among spectra.

if a series of EELS spectra are acquired from several standard specimens with known valence states, an empirical plot of these data serves as the reference for determining the valence state of the element present in a new compound.

The L_3/L_2 ratios for a few standard Co compounds are plotted in Fig. 2a. EELS spectra of Co–$L_{2,3}$ ionization edges were acquired from $CoSi_2$ (with Co^{4+}), Co_3O_4 (with $Co^{2.67+}$), $CoCO_3$ (with Co^{2+}) and $CoSO_4$ (with Co^{2+}). Fig. 2b shows a plot of the experimentally measured intensity ratios of white lines L_3/L_2 for Mn. The curves clearly show that the ratio of L_3/L_2 is very sensitive to the valence state of Co and Mn. This is the basis of our experimental approach for measuring the valence states of Co or Mn in a new material.

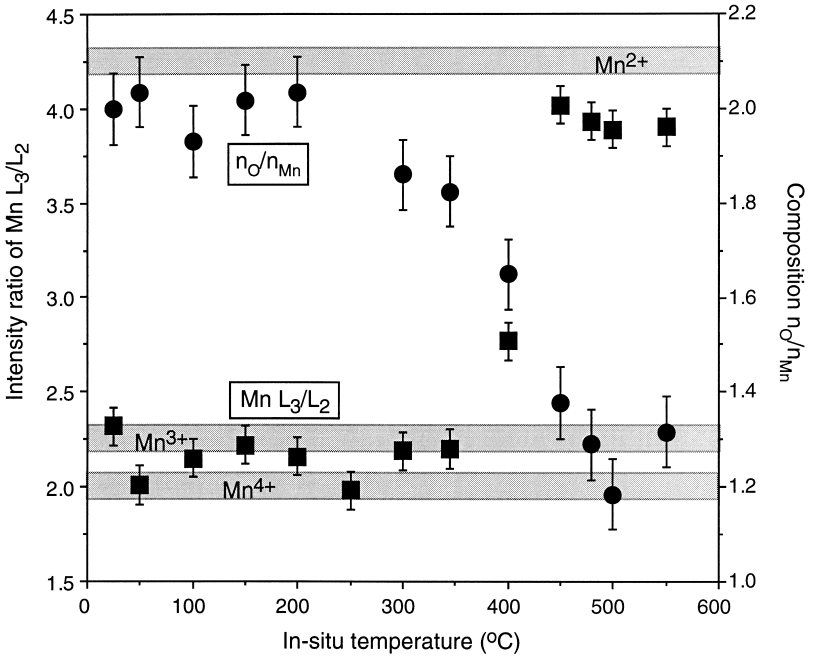

Fig. 4. An overlapped plot of the white line intensity ratio of Mn L_3/L_2 and the corresponding chemical composition of n_O/n_{Mn} as a function of the in situ temperature of the MnO_2 specimen based on EELS spectra, showing that the change in Mn valence state is accompanied with the variation in oxygen content.

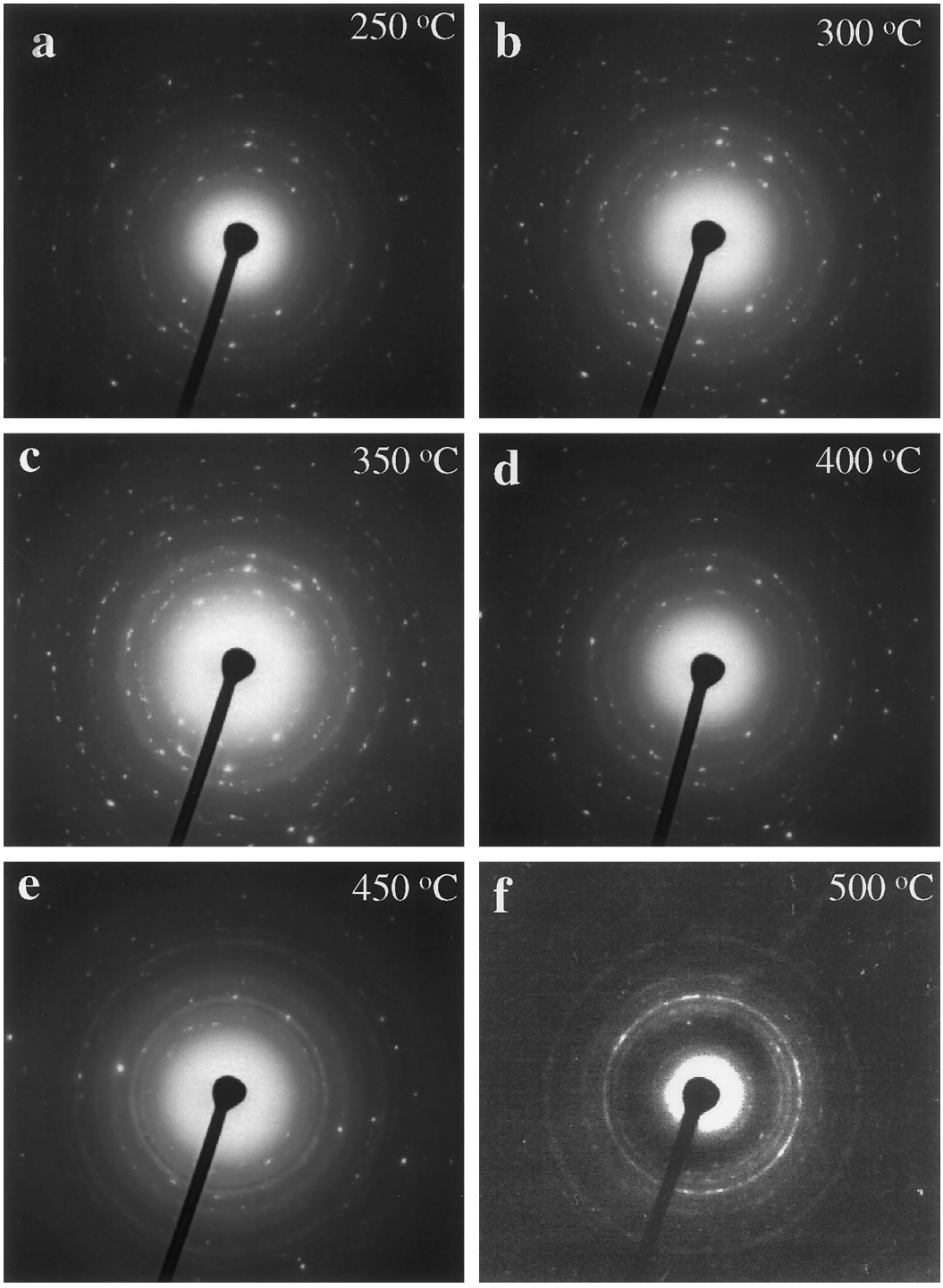

Fig. 5. A series of electron diffraction patterns recorded in situ from MnO_x during the thermal induced reduction of MnO_2 to Mn_3O_4. Note a small fraction of other phases do exist at the final stage. The final phase is identified in reference to the X-ray powder diffraction data.

3. In situ observation of valence state transition

For demonstrating the sensitivity and reliability of using white line intensity for the determination of the valence states in mixed valence compounds (Wang and Yin, 1998), the in situ reduction behavior of Co_3O_4 is examined first. A Gatan TEM specimen heating stage was employed to carry out the in situ EELS experiments, and the specimen temperature could be increased continuously from room temperature to 1000°C. The column pressure was kept at 3×10^{-8} Torr or lower during the in situ analysis.

Fig. 3 shows the Co L_3/L_2 ratio and the relative composition of n_O/n_{Co} for the same piece of crystal as the specimen temperature was increased. The specimen composition was

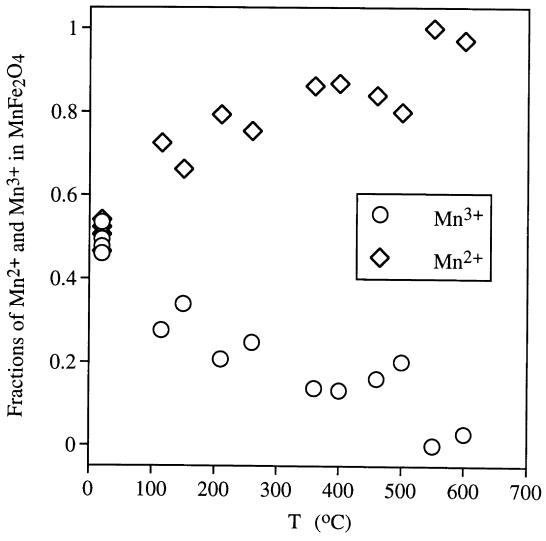

Fig. 6. Fractions of the Mn^{2+} and Mn^{3+} ions in $MnFe_2O_4$ measured by quantitatively fitting the experimental EELS spectra with the standard spectra of the oxides containing Mn^{2+} and Mn^{3+} ions. Five repeated measurements at 25°C are shown and give consistent result.

determined from the integrated intensities of the O–K and Co–$L_{2,3}$ ionization edges with the use of ionization cross-sections calculated using the SIGMAK and SIGMAL programs (Egerton, 1996). The L_3/L_2 ratios corresponding to Co^{2+} determined from the EELS spectra of $CoSO_4$ and $CoCO_3$ at room temperature, and $Co^{2.67+}$ obtained from Co_3O_4 are marked by shadowed bands, the widths of which represent experimental error and the variation among different compounds. The Co L_3/L_2 ratio and the composition, n_O/n_{Co}, simultaneously experience a sharp change at $T =$ 400°C. The chemical composition changes from $O : Co = 1.33 \pm 0.5$ to $O : Co = 0.95 \pm 0.5$ in accompany to the change of the average valence state of Co from 2.67+ to 2+ when the temperature is above 400°C.

The second experiment is performed on the reduction of MnO_2. Similarly, the plot of composition, n_O/n_{Mn} and white line intensity, Mn L_3/L_2, are shown in Fig. 4, where the shadowed bands indicate the white line ratios for Mn^{2+}, Mn^{3+} and Mn^{4+} as determined from the standard specimens of MnO, Mn_2O_3 and MnO_2, respectively. The reduction of MnO_2 occurs at 300°C. As the specimen temperature increases, the O/Mn ratio drops and the L_3/L_2 ratio increases, which indicates the valence state conversion of Mn from 4+ to lower valence states. At $T = 400$°C, the specimen contains the mixed valences of Mn^{4+}, Mn^{3+} and Mn^{2+}. As the temperature reaches 450°C, the specimen is dominated by Mn^{2+} and Mn^{3+} and the composition is $O/Mn = 1.3 \pm 0.5$, in correspondence of Mn_3O_4, which is consistent with the mixed valence of Mn cations and implies the uncompleted reduction of MnO_2.

To trace the relationship between the valence transition with the evolution of crystal structure, electron diffraction patterns were recorded in situ at different temperatures, as shown in Fig. 5. The crystal structure is MnO_2 (with rutile structure), and no visible change in crystallography is observed up to 400°C. From 400 to 450°C, the crystal structure experiences a rapid change from rutile to spinel, and the final phase at 500°C is identified to be dominated by Mn_3O_4, with the presence of a small fraction of other phases, consistent with the composition measured by EELS in Fig. 4.

Similar analysis has been performed for $MnFe_2O_4$ spinel structured nanocrystals (Wang and Kang, 1998; Zhang et al., 1998). The AB_2O_4 type of spinel structure has two types of cation lattice sites: a tetrahedral site A^{2+} formed by four nearest-neighbor oxygen anions, and an octahedral B^{3+} site formed by six oxygen anions. In $MnFe_2O_4$, the percentage of the A sites occupied by Fe specifies the degree of valence inversion. For a general case, the ionic structure of $MnFe_2O_4$ is written as $(Mn^{2+}_{1-x}Fe^{2+}_x)(Fe^{3+}_{1-y}Mn^{3+}_y)O_4$, in which the A and B sites can be occupied by either Mn or Fe. The magnetic property of this material depends strongly on the degree of inversion because the $Fe^{2+}_A - Fe^{3+}_B$ super-exchange interaction is much stronger than the $Mn^{2+}_A - Fe^{3+}_B$ interaction (Goodenough, 1971). An experimental measurement of the valence conversion of Mn in this material can provide concrete information on the distribution of Fe in the A and B sites, possibly leading to a better understanding of its magnetic property. Shown in Fig. 6 is the EELS measured fractions of the Mn^{2+} and Mn^{3+} ions in the $MnFe_2O_4$ specimen as a function of the in situ specimen temperature in TEM. The fraction was calculated by fitting the experimentally observed L_3 and L_2 EELS spectra by a linear summation of the spectra acquired from MnO and Mn_2O_3, and the coefficients for the linear combination give the percentages of the Mn ions of different valence states in the material. It is clear that the fractions of Mn^{2+} and Mn^{3+} ions at room temperature is 0.5:0.5, while a complete conversion into divalent Mn occurs at 600°C. These data explicitly illustrate the evolution in the valence state of the Mn ions, leading to a temperature dependent magnetic properties of $MnFe_2O_4$.

4. Quantification of oxygen vacancies in CMR oxides

The CMR magnetic oxides ($La_{1-x}A_xMnO_3$ and $La_{1-x}A_xCoO_3$) have a perovskite-type crystal structure with ferromagnetic ordering in the a–b planes and antiferromagnetic ordering along the c-axis. The partial substitution of trivalent La^{3+} by divalent element A^{2+} is balanced by the conversion of Mn valence states between Mn^{3+} and Mn^{4+} (or Co^{3+} and Co^{4+} for Co) and the creation of oxygen vacancies as well. This valence state conversion of Mn was proposed by Jonker and van Santen (1953), and the ionic structure of $La_{1-x}A_xMnO_{3-y}$ is

$$La^{3+}_{1-x}A^{2+}_xMn^{3+}_{1-x+2y}Mn^{4+}_{x-2y}O^{2-}_{3-y}V^{O}_y \quad (1)$$

where V^O_y stands for the fraction of oxygen vacancies. This

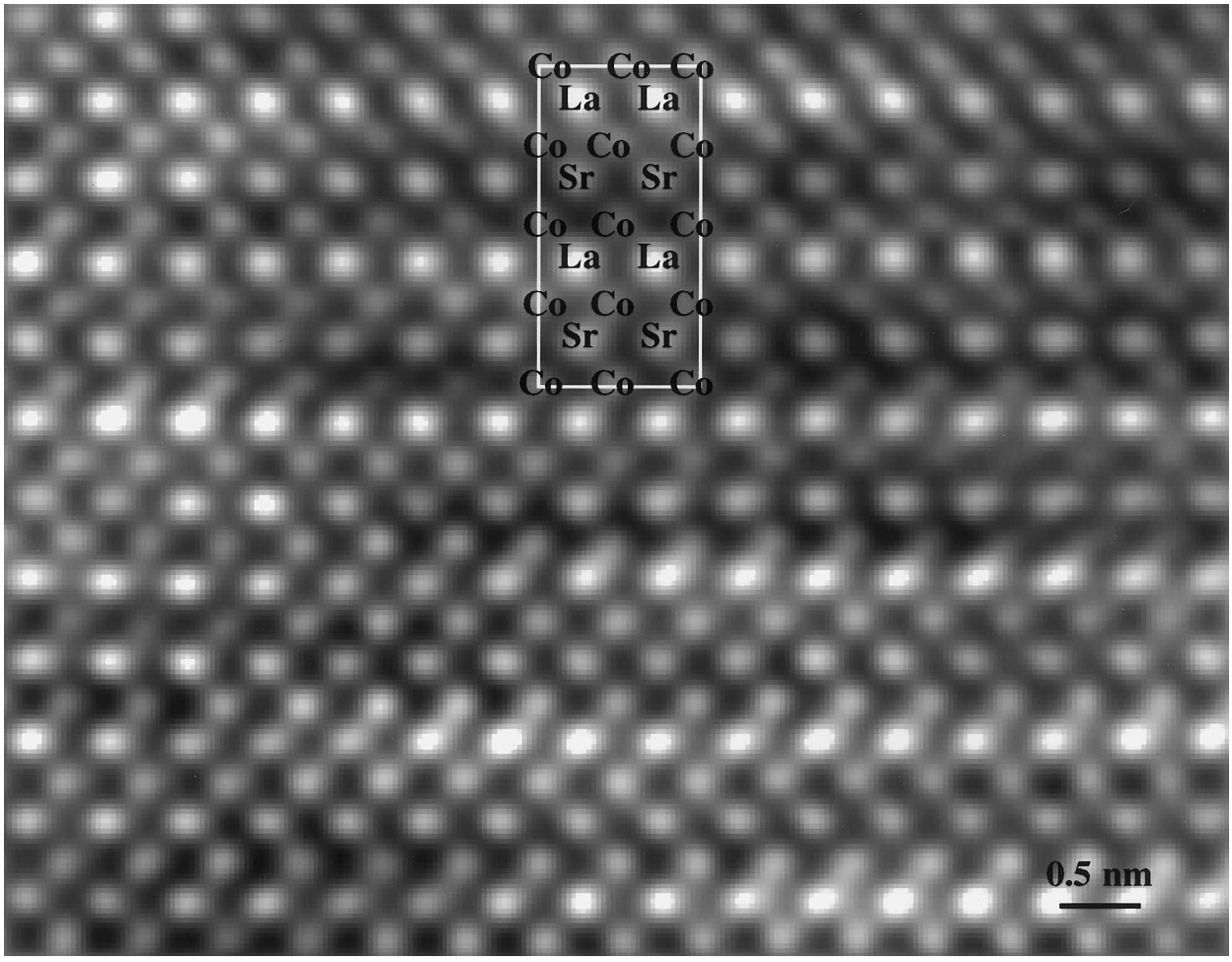

Fig. 7. A high-magnification [100] TEM image of $La_{0.5}Sr_{0.5}CoO_{2.25}$, where the white spots correspond to the projected atom columns with La the strongest contrast, Sr strong, and Co weak and oxygen invisible. The rectangular box indicates the [100] projection of the unit cell. The image was recorded at 300 kV.

ionization formula is proposed with an assumption that there is no residual charge trapped in the vacancy sites.

In practice, quantifying of oxygen vacancies is a challenge to the existing microscopy techniques although X-ray and neutron diffuse scattering can be used to determine vacancies in large bulk single crystalline specimens. Moreover, for thin films grown on a crystalline substrate the diffraction analysis may be strongly affected by the defects at the substrate–film interface and the surface disordering. In this section, we show the application of EELS for quantifying oxygen vacancies.

From Eq. (1), the mean valence state of Mn is

$$\langle \mathrm{Mn} \rangle_{\mathrm{vs}} = 3 + x - 2y. \tag{2}$$

The amount of doping x is usually known from energy dispersive X-ray microanalysis. The $\langle \mathrm{Mn} \rangle_{\mathrm{vs}}$ can be determined using EELS based on the white line intensity as illustrated in Section 2. Therefore, the content of oxygen vacancies y can be obtained (Wang et al., 1997).

For a $La_{0.67}Ca_{0.33}MnO_{3-y}$ thin film grown by metal-organic chemical vapor deposition, the L_3/L_2 ratio was measured to be $2.05 - 2.17$, thus, the average valence state of Mn is 3.2–3.5 according to the empirical plot shown in Fig. 2b. Substituting this value into Eq. (2) for $x = 0.33$, yields $y \leq 0.065$, which is equivalent to less than 2.2 at% of the oxygen content. At the maximum oxygen vacancy $y_{\max} = 0.065$, the atom ratio of Mn^{4+} to Mn^{3+} in the specimen is 0.25, thus, the charge introduced by Mn valence conversion is $(x - 2y) = 0.2^{+}$, the charge due to oxygen vacancy is $2y = 0.13^{-}$, which means that 60% of the residual charge introduced by Ca doping is balanced by the conversion of Mn^{3+} to Mn^{4+} and 40% by oxygen vacancies. Therefore, a small percentage of oxygen vacancy can introduce a large effect in balancing the charge. Quantification of oxygen vacancies by this technique may have higher sensitivity than the conventional EELS microanalysis for such a small percentage of vacancies.

5. Refining the crystal structures of non-stoichiometric oxides

$La_{0.5}Sr_{0.5}CoO_{3-y}$ is a magnetic oxide that has potential applications in fuel cells and ionic conductivity. The cation

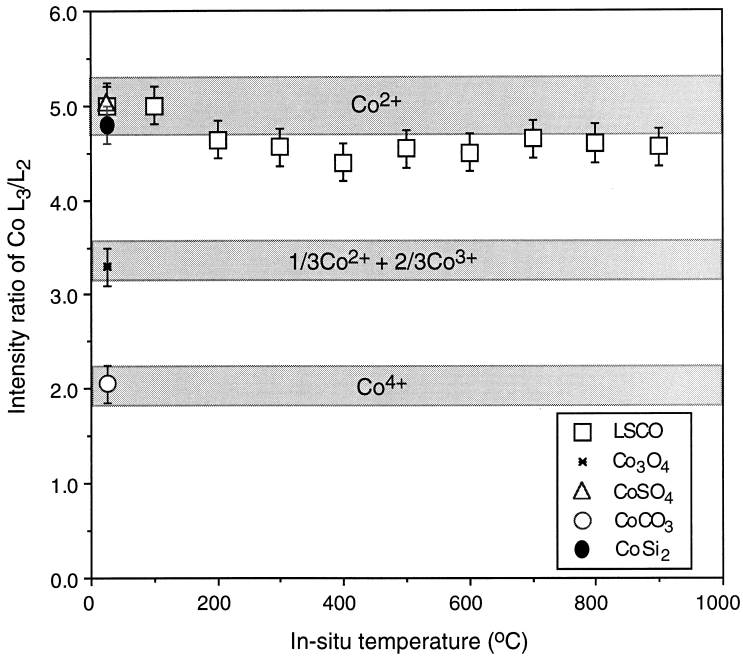

Fig. 8. A relationship between the Co L_3/L_2 intensity ratio and the in situ temperature of $La_{0.5}Sr_{0.5}CoO_{2.25}$, proving the divalent state of Co.

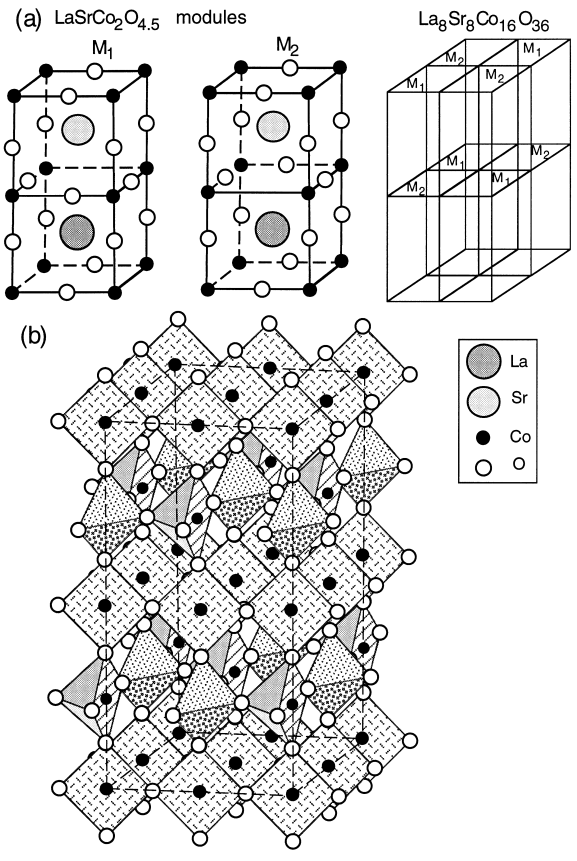

Fig. 9. (a) Two anion deficient modules of $LaSrCo_2O_{4.5}$, and the corresponding stacking to form a complete unit cell of $La_8Sr_8Co_{16}O_{36}$ (or $La_{0.5}Sr_{0.5}CoO_{2.25}$). (b) The 3D model of the structure proposed for $La_8Sr_8Co_{16}O_{36}$, where the Co with coordination numbers of 4, 5 and 6 are shown and the La and Sr cations are omitted for clarity.

structure of this material can be determined by high-resolution TEM. Fig. 7 shows a high-magnification TEM image of the $La_{0.5}Sr_{0.5}CoO_{3-y}$ crystal oriented along [100], exhibiting *c*-axis directional anisotropy structure. This type of images can directly give the projected position of the cations in the unit cell (Wang and Zhang, 1995,1996), while no information can be provided about the distribution of oxygen anions. The image is also insensitive to the valence state of Co.

For perovskite structured oxides, the oxygen deficiency, if any, is rather small, thus, the quantification of oxygen content is difficult using either EELS or EDS microanalysis technique. Alternatively, one can use EELS to measure the mean valence state of Co, then applying the result to determine the oxygen deficiency. For the specimen $La_{0.5}Sr_{0.5}CoO_{3-y}$ used to record the TEM image given in Fig. 7, the mean valence of Co is determined to be 2+, hence the ionic structure of this crystal is

$$La^{3+}_{0.5}Sr^{2+}_{0.5}Co^{2+}O^{2-}_{2.25}V^{O}_{0.75}.$$

To confirm that the valence state of Co in $La_{0.5}Sr_{0.5}CoO_{3-y}$ is 2+, the in situ EELS measurement is carried out. As the specimen temperature increases, a reduction of oxide would lead to a reduction in the valence state of Co if the Co has a valence state other than 2+. Fig. 8 shows the experimentally measured L_3/L_2 ratio as a function of the specimen temperature. The partial pressure of oxygen is rather low in TEM, thus, oxidation is unlikely to occur based on our studies of MnO_x and CoO_y (see Figs 3 and 4). It is anticipated that a significant change in L_3/L_2 ratio would be observed if the

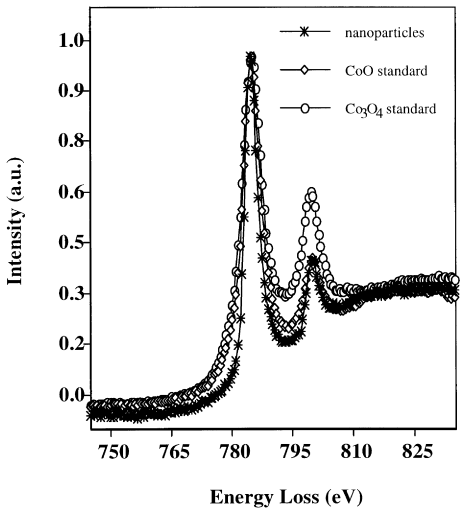

Fig. 10. A comparison of EELS spectra of Co–$L_{2,3}$ ionization edges acquired from Co_3O_4 and CoO standard specimens and the as-synthesized nanocrystals, proving that the valence state of Co is 2+ in the nanocrystals. The full width at half maximum of the white lines for the Co_3O_4 and CoO standards is wider than that for the nanocrystals, possibly due to size effect.

valence state of Co changes. In contrast, the experimentally observed L_3/L_2 ratio has little dependence on the temperature and the ratio remains in the Co^{2+} range even when the oxide is totally changed crystallographically at 900°C (Yin and Wang, 1998). Therefore, the valence state of Co is undoubtedly 2+. This information is important to confirm the reliability of the structural mode proposed above. The surprisingly high stability of $La_{0.5}Sr_{0.5}CoO_{2.25}$ is likely to be very useful for ionic conductor because of the maximum density of oxygen vacancies.

Quantitative determination of the structure of this crystal needs the support of data from X-ray diffraction, electron diffraction and HRTEM imaging. More importantly, the valence state of Co measured by EELS is indispensable for refining the crystal structure because the compound is chemically non-stoichiometric. From electron diffraction, we also know that the oxygen vacancies are ordered in the crystal. Fig. 9 gives the structural model proposed based on all of the known structure information (Wang and Yin, 1998). The unit cell is made of two fundamental structural modules M_1 and M_2 and its crystal structure is $La_8Sr_8Co_{16}O_{36}$, while the entire structure still preserves the characteristics of perovskite framework and is a superstructure induced by an ordered structure of oxygen vacancies. The polyhedra formed by the oxygen anions that coordinate a Co atom can be a planar square (coordination number (CN) = 4), a square-based pyramid ($CN = 5$), or a octahedron ($CN = 6$). These modules are required to balance the chemical structure of the crystal.

6. Identification of the structure of nanoparticles

Determination of the crystal structure of nanoparticles is a challenge particularly when the particles are smaller than 5 nm. The intensity maxim observed in the X-ray or electron

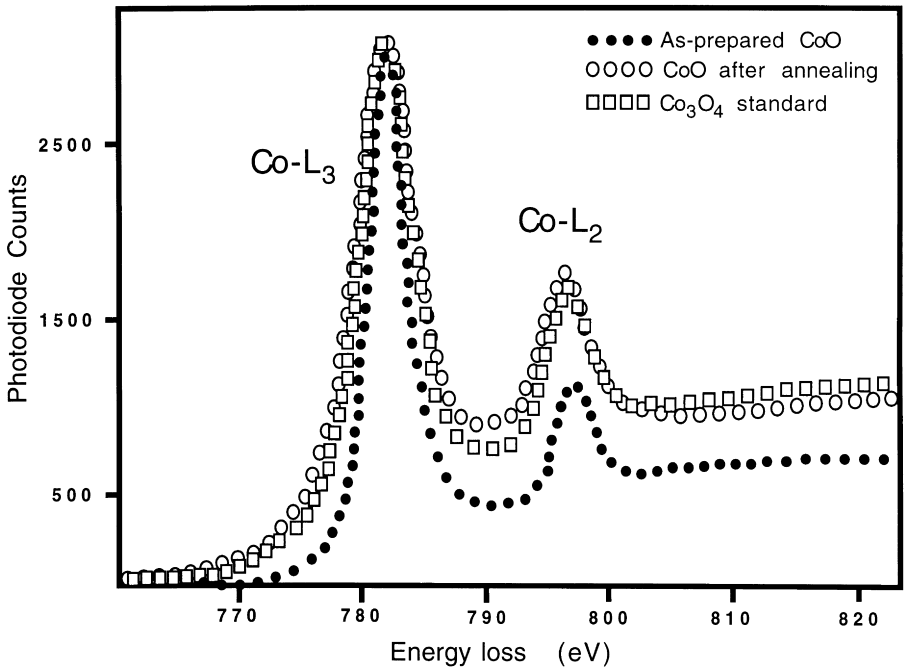

Fig. 11. A comparison of EELS spectra of Co–$L_{2,3}$ ionization edges acquired from the as-prepared CoO nanoparticles, post-annealed CoO in oxygen atmosphere, and the Co_3O_4 standard, proving that the CoO nanoparticles of 5 nm in size have been transformed into Co_3O_4 after annealing at 250°C for 18 h in oxygen.

diffraction patterns of such small particles are broadened due to the crystal shape factor, greatly reducing the accuracy of structure refinement. The quality of the high-resolution TEM images of the particles is degraded because of the strong effect from the substrate. This difficulty arises in our recent study of CoO nanocrystals whose shape is dominated by tetrahedral of sizes smaller than 5 nm. Electron diffraction indicates that the crystal has a NaCl type of structure. To confirm the synthesized nanocrystals are CoO, EELS is used to measure the valence state of Co. Fig. 10 shows a comparison of the spectra acquired from Co_3O_4 and CoO standard specimens and the synthesized nanocrystals. The relative intensity of the Co–L_2 to Co–L_3 for the nanocrystals is almost identical to that for CoO standard, while the Co–L_2 line of Co_3O_4 is significantly higher, indicating that the Co valence in the nanocrystals is 2+, confirmed the CoO structure of the nanocrystals (Yin and Wang, 1997b).

Ex situ annealing of the CoO nanoparticles in an oxygen atmosphere is likely to convert the particles into Co_3O_4. This structural evolution is verified by EELS, as shown in Fig. 11, where the EELS spectra acquired from the as-synthesized CoO nanocrystals, a standard bulk Co_3O_4 specimen, and the post ex situ annealed nanoparticles. The spectrum of the post-annealed nanoparticles fits very well with that of Co_3O_4, strongly support the conversion from CoO to Co_3O_4.

7. Summary

For characterizing advanced and functional materials that usually contain cations with mixed valences, EELS is a very powerful approach with a spatial resolution higher than any other spectroscopy techniques available. Based on the intensity ratio of white lines, it has been demonstrated that the valence states of Co and Mn in oxides can be determined quantitatively. This information is important in studying valence transition in oxides.

EELS is most sensitive to the divalent and trivalent Mn and Co ions, while the difference between Mn^{3+} and Mn^{4+} or Co^{3+} and Co^{4+} is small, leading to a larger error in identification of the valence state because of experimental error. The only possible solution is to acquire high quality EELS spectra. From the experimental point of view, we found that Mn and Co are the only transition metal elements whose white line ratios are most sensitive to valence state variation, while the white lines of Fe are almost independent of its valence states. Therefore, more theoretical research is required to explore the origin of white lines.

Acknowledgements

We are grateful to Drs J. Zhang and Z.J. Zhang for providing the $La_{0.5}Sr_{0.5}CoO_{3-y}$ and the $MnFe_2O_4$ specimens, respectively. This work was supported by NSF (DMR-9632823 and DMR-9733160).

References

Botton, G.A., Appel, C.C., Horsewell, A., Stobbs, W.M., 1995. Quantification of the EELS near-edge structures to study Mn doping in oxides. J. Microsc. 180, 211–216.

Egerton, R.F., 1996. Electron Energy-Loss Spectroscopy in the Electron Microscope, 2. Plenum Press, New York.

Fortner, J.A., Buck, E.C., 1996. The chemistry of the light rare-earth elements as determined by electron energy-loss spectroscopy. Appl. Phys. Lett. 68, 3817–3819.

Goodenough, J.B., 1971. Metallic oxides. Prog. Solid State Chem. 5, 145–399.

von Helmolt, R., Wecker, J., Holzapfel, B., Schultz, L., Samwer, K., 1994. Giant negative magnetoresistance in perovskitelike $La_{2/3}Ba_{1/3}MnO_x$ ferromagnetic films. Phys. Rev. Lett. 71, 2331–2334.

Jin, S., Tiefel, T.H., McCormack, M., Fastnacht, R.A., Ramech, R., Chen, L.H., 1994. Thousandfold change in resistivity in magnetoresistive La–Ca–Mn–O films. Science 264, 413–415.

Jonker, G.H., van Santen, J.H., 1953. Magnetic compounds with perovskite structure. III. Ferromagnetic compounds of cobalt. Physica 19, 120–130.

Krivanek, O.L., Paterson, J.H., 1990. ELNES of 3d transition-metal oxides. I. Variations across the periodic table. Ultramicroscopy 32, 313–318.

Kurata, H., Colliex, C., 1993. Electron-energy loss core-edge structures in manganese oxides. Phys. Rev. B 48, 2102–2108.

Lloyd, S.J., Botton, G.A., Stobbs, W.M., 1995. Changes in the iron white-line ratio in the electron energy-loss spectrum of iron–copper. J. Microsc. 180, 288–293.

Mansot, J.L., Leone, P., Euzen, P., Palvadeau, P., 1994. Valence of manganese, in a new oxybromide compound determined by means of electron energy loss spectroscopy. Microsc. Microanal. Microstruct. 5, 79–90.

Morrison, T.I., Brodsky, M.B., Zaluzec, N.J., Sill, L.R., 1985. Iron d-band occupancy in amorphous Fe_xGe_{1-x}. Phys. Rev. B 32, 3107–3111.

Pearson, D.H., Fultz, B., Ahn, C.C., 1988. Measurement of 3d state occupancy in transition metals using electron energy-loss spectroscopy. Appl. Phys. Lett. 53, 1405–1407.

Pearson, D.H., Ahn, C.C., Fultz, B., 1993. White lines and d-electron occupancies for the 3d and 4d transition metals. Phys. Rev. B 47, 8471–8478.

Pease, D.M., Bader, S.D., Brodsky, M.B., Budnick, J.I., Morrison, T.I., Zaluzec, N.J., 1986. Anomalous L3/L2 white line ratios and spin pairing in 3d transition metals and alloys: Cr metals and Cr20Au80. Phys. Lett. A 114, 491–494.

Thole, B.T., van der Laan, G., 1988. Branching ratio on X-ray absorption spectroscopy. Phys. Rev. B 38, 3158–3169.

Wang, Z.L., Kang, Z.C., 1998. Functional and Smart Materials—Structural Evolution and Structure Analysis, Plenum Press, New York.

Wang, Z.L., Yin, J.S., 1998. Cobalt valence and crystal structure of $La_{0.5}Sr_{0.5}CoO_{2.25}$. Philos. Mag. B 77, 49–65.

Wang, Z.L., Zhang, J., 1995. Microstructure of conductive $La_{1-x}Sr_xCoO_3$ grown on MgO(001). Philos. Mag. A 72, 1513–1529.

Wang, Z.L., Zhang, J., 1996. Tetragonal domain structure magnetoresistance of $La_{1-x}Sr_xCoO_3$. Phys. Rev. B 54, 1153–1158.

Wang, Z.L., Yin, J.S., Jiang, Y.D., Zhang, J., 1997. Studies of Mn valence conversion and oxygen vacancies in $La_{1-x}Ca_xMnO_{3-y}$ using electron energy-loss spectroscopy. Appl. Phys. Lett. 70, 3362–3364.

Wang, Z.L., Yin, J.S., Zhang, J.Z., Mo, W.D., 1997. In-situ analysis of valence conversion in transition metal oxides using electron energy-loss spectroscopy. J. Phys. Chem. B 101, 6793–6798.

Yin, J.S., Wang, Z.L., 1997. Ordered self-assembling of tetrahedral oxide nanocrystals. Phys. Rev. Lett. 79, 2570–2573.

Yin, J.S., Wang, Z.L., 1998. In-situ EELS analysis of cobalt valence in $La_{1-x}Sr_xCoO_{3-y}$, Proceedings of the Microscopy Society America, Microscopy Society of America, Cleveland, OH.

Yuan, J., Gu, E., Gester, M., Bland, J.A.C., Brown, L.M., 1994. Electron energy-loss spectroscopy of Fe thin-films on GaAs(001). J. Appl. Phys. 75, 6501–6503.

Zhang, Z.J., Wang, Z.L., Chakoumakos, B.C., Yin, J.S., 1998. Temperature dependence of cation distribution and oxidation state in magnetic Mn–Fe ferrite nanocrystals. J. Am. Chem. Soc. 120, 1800–1804.